Nanosized zeolite beta - Determining the safety of usage by zebrafish Danio rerio embryos

Ana Palčić, Sanja Babić, Aleksandra Maršavelski, Maja Galić, Natalija Topić Popović, Ivančica Strunjak Perović, Rozelindra Čož-Rakovac, Josip Bronić, Valentin Valtchev

Nanosized zeolite beta - determining the safety of usage by zebrafish *Danio rerio* embryos

Ana Palčić[a,1,*], Sanja Babić[b,c,1,**], Aleksandra Maršavelski[d], Maja Galić[b,c], Natalija Topić Popović[b,c], Ivančica Strunjak Perović[b,c], Rozelindra Čož-Rakovac[b,c], Josip Bronić[a], Valentin Valtchev[e]

[a]Ruđer Bošković Institute, Division of Materials Chemistry, Laboratory for Synthesis of New Materials, Bijenička cesta 54, Zagreb, Croatia

[b]Ruđer Bošković Institute, Division of Materials Chemistry, Laboratory for Aquaculture Biotechnology, Bijenička cesta 54, Zagreb, Croatia

[c]Center of Excellence for Marine Bioprospecting (BioProCro), Ruđer Bošković Institute, Bijenička cesta 54, Zagreb

[d]University of Zagreb, Faculty of Science, Department of Chemistry, Horvatovac 102a, Zagreb, Croatia

[e]Normandie Univ, ENSICAEN, UNICAEN, CNRS, Laboratoire Catalyse et Spectrochimie, 6 Boulevard Maréchal Juin, Caen, France

[1]Equal contribution

[*]Corresponding author

[**]Corresponding author

E-mail addresses: ana.palcic@irb.hr (A. Palčić), sanja.babic@irb.hr (S. Babić)

Keywords

Nanozeolites; Organic structure directing agents; Nanotoxicology; Zebrafish embryotoxicity test; Molecular docking

Highlights

- Zeolite nanoparticles showed no impact on zebrafish embryonic development
- Tetraethylammonium cations tend to leach from the zeolite *BEA framework
- Oxidative stress leads to hatching delay in zebrafish exposed to non-calcined zeolite samples and TEAOH

Abstract

Zeolites are materials widely used in many fields of human activities. Furthermore, new potential applications constantly emerge, so understanding their possible impact on the environment is necessary. Within this study, the potential toxicity of nanosized particles (140 and 600 nm) of a widely used zeolite beta was evaluated using zebrafish *Danio rerio* embryos. Embryotoxicity test, with an emphasis on sublethal changes, was performed on three concentrations of each nanosized zeolite sample (calcined and non-calcined). Toxicity of tetraethylammonium species (TEA) present in non-calcined zeolite samples was also investigated using experimental and computational approaches. The data suggest that non-calcined zeolites and tetraethylammonium hydroxide (TEAOH) itself caused hatching failure, but also initiated oxidative stress and apoptosis. Such observation confirmed certain TEA leaching from the zeolite framework, thus impacting embryonic development. Since molecular docking and molecular dynamics simulations did not show TEA inhibition of the hatching enzyme ZHE1 and the ROS formation was detected using fluorescence microscopy, it was concluded that oxidative stress is the major mechanism underlying the toxicity of non-calcined samples and TEAOH. Contrary to that, calcined zeolite nanoparticles, although having a strong interaction with the chorion and subsequently with the embryos, did not show a negative impact on zebrafish survival/development. Such a comprehensive study pinpointed zeolite nanoparticles as safe materials and opened the door for their application.

1.0. Introduction

Zeolites are crystalline microporous tectosilicate materials built of tetrahedra with central T atom (T=Si, Al, Ti, P, B, Ge, Ga, etc.) and surrounded by oxygen atoms at vertices [1]. Depending on the arrangement of the tetrahedra, numerous tridimensional frameworks with the system of voids and channels of different sizes can get formed. Currently, there are over two million possible hypothetical zeolite structures and 234 approved zeolite frameworks found in nature and prepared in the laboratories [2,3]. Due to their particular properties such as tunable hydrophobicity, acidity, ion-exchange, morphology, size, and molecular sieving ability, zeolites are widely used in many industrial processes and everyday life [1,4,5]. The used materials range from all silica materials to low silica zeolites, from titanium-containing zeolites to silicoaluminophosphates. Synthetic zeolites are mainly used as catalysts in (petro)chemical industry, ion-exchangers in detergents and as molecular sieves in numerous separation processes. They are also employed in wastewater treatment, water purification, odor removal,

agriculture, medicine, solar cells, refrigeration, etc [6]. Furthermore, several studies reported a rise of zeolites application for biomedical purposes, i.e. as hosts for the encapsulation and delivery of anti-cancer drugs, but also for prevention of uncontrolled bleeding [7].

Zeolite beta is a member of the "Big Five" zeolites that dominate most of the commercial zeolite production for catalysis. It is applied as a catalyst in various industrial processes such as isomerization of waxes, Friedel Crafts reactions (alkylation and acylation), in the stereoselective Meerwein-Ponndorf-Verley reduction of ketones and for the tetrahydropyranylation of alcohols and phenols [8,9]. Zeolite beta is also employed as a catalyst in the cumene and ethylbenzene technologies at ENI [4]. Lately, Zr-, Hf- and Sn-beta zeolite materials are increasingly tested as catalysts for biomass valorization [10]. Similarly to other fields, there has been intensive development in the synthesis and application of nanosized zeolites [11,12]. Namely, nanosized zeolites have been shown to have good performance in water electrolysis [13], can act as ultraviolet shielding material [14], and sensors [15]. Due to their remarkable properties and the fact that they can be supplied in various forms (from colloidal suspensions, thin films, to membranes and self-supported morphologies), it can be assumed that nanosized zeolites will be involved in many scientific fields, industry, and consequently will become ubiquitous in many everyday products [6].

One of the most challenging issues in the field of nanotechnology is environmental health and safety, which is only achievable through consideration of the properties of engineered nanomaterials that could pose a hazard to the environment, but also to environmental organisms and human beings [16]. There are many articles dealing with the synthesis of nanosized zeolites [6,11], however, only a few studies investigated the impact of nanosized zeolites mainly by assessing zeolite cytotoxicity and neglecting a whole organism level [7,17,18]. Hence, it is necessary to carry out extensive studies that involve testing of different materials in terms of their chemical composition and framework type, as well as materials having different properties in terms of their surface area, crystal size and shape, porosity, hydrophobicity, acidity, and ion-exchange capacity. Furthermore, it is indispensable to establish the possible effects of nanosized zeolites on the specific ecosystems and living organisms.

With that goal, zebrafish *Danio rerio* - a promising small animal model that can be used in developmental, pharmacological, genetic and toxicological research, was employed as a model organism. Its small size, high fecundity, rapid development, optical transparency during the whole embryonic development, availability of genomic data and genetic similarity to humans, are just some of the reasons that enabled the use of an entire living organism (*in vivo*) in standardized *in vitro* format [19,20]. This ability to position zebrafish as a bridge between cell-

based tools and other *in vivo* models allows not only the extrapolation of the data across physiological targets and vertebrate taxa, but could also serve as a base of sustainable chemistry [19]. Nowadays, zebrafish are being used as *in vivo* platforms to study toxic effects and determine environmental risk assessment of pharmaceuticals [21], heavy metals [22], pesticides [23,24], microplastics [25,26], environmental samples [27–29], but also nanoparticles [30–32]. Herein we provided the comprehensive insight into the impact of two nanosized zeolite beta particles sizes on zebrafish *Danio rerio* embryonic development. For the preparation of nanosized zeolite beta the presence of organic structure-directing agent (OSDA), tetraethylammonium hydroxide (TEAOH), is indispensable [5]. Namely, the TEA^+ cations assemble the porous zeolite network and thus are located within zeolite voids, i.e. distributed throughout the crystal. Prior to any application, OSDA has to be removed from the pores by calcination of the samples [33]. For this reason, both calcined and non-calcined zeolite materials have been investigated. Firstly, the physicochemical characterization of the prepared samples has been performed by a set of complementary techniques. Subsequently, *D. rerio* embryos were exposed to calcined and non-calcined nanosized zeolite samples, but also to the TEAOH in concentrations corresponding to the ones present in zeolite samples. During zebrafish embryotoxicity test (ZET) special attention was given to sublethal effects, which were supplemented with molecular modeling in order to elucidate the mechanism of the observed effect of delayed hatching. The additional extent to the ZET test was done in terms of quantifying toxic effects at the cellular level by recording apoptotic cells and reactive oxygen species (ROS) formation. Taken together, multiple biological endpoints used in this study within one model organism proved to be a valuable and reliable basis for determining the impact of zeolite beta nanoparticles.

2.0. Materials and methods

2.1. Chemicals

Tetraethylammonium hydroxide (35% water solution; TEAOH), fumed silica (99.80%), aluminium isopropoxide (98%), Ludox HS-30, acridine orange (AO), 2′,7′-dichlorofluorescin diacetate (DFC), ethyl 3-aminobenzoate methanesulfonate salt (MS-222), as well as calcium chloride dihydrate (p.a.), magnesium sulfate heptahydrate (98%) sodium bicarbonate (p.a.) were obtained from Sigma Aldrich (Germany). Potassium hydroxide (pellets, 85%) and sodium hydroxide (pellets, 98%) were obtained from Kemika (Croatia), while sodium aluminate (54% Al_2O_3) was purchased from Honeywell Riedel-de Haën AG (Germany). Artificial water was

prepared by dissolving 294.0 mg L^{-1} $CaCl_2 \times 2\ H_2O$, 123.3 mg L^{-1} $MgSO_4 \times 7H_2O$, 63.0 mg L^{-1} $NaHCO_3$, and 5.5 mg L^{-1} KCl (Sigma Aldrich, Germany) in deionized water.

2.2. Preparation and characterization of zeolite nanoparticles

Sample BEA-140 was prepared according to Landau et al. [34]. The needed amount of aluminium isopropoxide was dissolved in TEAOH. Freeze-dried Ludox HS-30 was added to TEAOH and stirred for 10 minutes by using a magnetic stirrer. Two components were mixed and stirred for 10 minutes and subsequently transferred into an oven preheated at 100°C. The final molar oxide composition of the synthesis mixture was $0.35Na_2O{:}0.5Al_2O_3{:}25\ SiO_2{:}9TEAOH{:}295H_2O$. The crystalline sample was recovered after 7 days of hydrothermal treatment. The solid phase has been washed with deionized water repeatedly until pH 7 by centrifugation and dried by freeze-drying. Organic structure-directing agent (TEAOH) was removed by calcination of the dried powder at 550°C for 6 h in static air (BEA-140-calc).

Sample BEA-600 was prepared by mixing of the suspension of fumed silica in a solution of KCl in H_2O and TEAOH together with the solution of sodium aluminate in water and KOH. The molar oxide composition was $1.23K_2O{:}1.23Na_2O{:}1Al_2O_3{:}50SiO_2{:}25TEAOH{:}745H_2O$ [35]. After 10 minutes of agitation, the synthesis mixture was treated for 30 h at 140°C. The solid phase was centrifuged repeatedly in deionized water until pH 7 and dried by freeze-drying. Organic structure directing agent was removed by calcination of the dried powder at 550°C for 6 h in static air. In this way, the sample BEA-600-calc was obtained.

Powder X-ray diffraction (XRD) data of the solid sample were collected on a Phillips PW3710 diffractometer with CuK_α source. Thermogravimetric measurements (TG) of the solid samples were performed using a Setaram Setsys TGA instrument, heating rate 5°C min^{-1} in air. The size of the crystals was measured employing Malvern Zetasizer Nano ZS. The powders were dispersed both in deionized and artificial water and measured as such. Scanning electron micrographs were obtained by employing an FE-SEM JEOL JSM-7000F microscope (SEM). For transmission electron microscopy (TEM) imaging, a small amount of the sample was dispersed in ethanol. After being treated by ultrasonication, one drop of the sample mixture was taken from the ethanol solution and transferred to a copper grid covered by a holey carbon film. Transmission electron microscope JEOL JEM-3010 was used for TEM studies. A Gatan 794 CCD camera was used for recording transmission electron microscopy images.

Zeolite suspensions were prepared in three concentrations: - 25, 50 and 100 µg L^{-1} by dispersing in artificial water. Prior to embryotoxicity test samples were aerated to oxygen saturation. TEAOH solutions in artificial water having concentrations 4.5, 9 and 18 µg L^{-1} were tested as

well. These concentrations correspond to the average amount of organic species within the zeolite material (18 wt% as measured by TG).

2.3. Toxicity testing

2.3.1. Ethics statement

Animal housing and spawning were performed in aquaria units approved by the Croatian Ministry of Agriculture and according to the Directive 2010/63/EU on the protection of animals used for scientific purposes [36]. All experiments in this study were conducted on the non-protected embryonal stages (up to 72 hpf), which do not require permission by animal welfare commissions [36].

2.3.2. Zebrafish maintenance and egg production

Zebrafish *D. rerio* (wildtype) were maintained under controlled laboratory conditions, described in detail in our previous works [27]. In the evening, males and females were sequentially added into the iSpawn-S Benchtop Size Breeding System (Techniplast, Italy) and were kept separated by a divider. The next day, the divider was removed and the spawning platform lifted to initiate the spawning. After spawning, eggs were collected within 20 min using 800 μm mesh and were rinsed with artificial water (AW) in order to remove the debris.

2.3.3. Zebrafish embryotoxicity test

Exposure was performed by the ZET test [37]. Fertilized eggs from 4- to 64- blastomeres were selected under a stereomicroscope (PRO-LUX, Croatia) and transferred individually into 24-well plates containing 1 mL of calcined and non-calcined BEA suspensions (25, 50, 100 μg mL^{-1}) and TEAOH (4.5, 9 and 18 μg mL^{-1}). The artificial water was used as negative control. Plates were kept at 27.0±0.5°C with a 14/10 h light/dark cycle in the Innova 42 incubator shaker (New Brunswick). Daily, 30% of the test sample volume (nano-zeolites, TEAOH, artificial water) was replaced in order to ensure constant conditions - minimize/prevent exposure concentration change during the assay, but also to preserve the optimal dissolved oxygen concentration necessary for zebrafish normal development. Prior to solution replacement, nano-zeolitesuspensions were dispersed by sonicator in order to prevent agglomeration (Bandelin Sonorex). The test was conducted with 10 embryos in three independent replicas. Up to 72 hours post-fertilization (hpf) lethal and sub-lethal effects were estimated [27,37].

205 **2.3.3.1. Reactive oxygen species assay**

206 For identification of ROS induced by nano-zeolites, embryo staining with DCFDA was
207 performed [38]. DCFDA is commonly used in detecting oxidative stress in zebrafish embryos
208 because it is a cell-permeable and ROS-reactive reagent. After 72 hpf larvae exposed to the
209 highest concentration of each tested sample (100 and 18 μg mL^{-1} of nano-zeolite suspensions
210 and TEAOH, respectively) were rinsed three times with AW and exposed to 10 μM DCFDA in
211 darkness. After 1 h of incubation, larvae were rinsed three times with AW and anesthetized
212 with 0.03% MS-222 for 2 min. ROS formation was observed in DCFDA-stained fish using a
213 fluorescence microscope (Olympus® BX51 light binocular microscope equipped with the
214 Microsoft® AnalySIS Soft Imaging System Software) with a green fluorescent filter. Semi-
215 quantitative analysis was performed using ImageJ software (n=10). In order to detect possible
216 interferences of nano-zeolites with the ROS assay (e.g. binding of assay components,
217 fluorescence interference due to the same wavelength of the assay dye and tested samples),
218 interference controls were run in parallel [39].
219
220 **2.3. 3.2. Apoptosis assay**

221 To investigate the potential apoptosis in the whole zebrafish larvae, nucleic acid-selective dye,
222 AO was used [38]. After 72-h exposure to nano-zeolite suspensions (100 μg mL^{-1}) and TEAOH
223 (18 μg mL^{-1}), zebrafish larvae were rinsed three times with AW and incubated in AO (5 μg
224 mL^{-1} in AW) for 30 min in darkness. After the incubation period, fish were rinsed three times
225 with AW. The AO-stained fish were anesthetized with 0.03% MS-222 for 2 min and observed
226 under a fluorescence microscope (Olympus® BX51 light binocular microscope equipped with
227 the Microsoft® AnalySIS Soft Imaging System Software) with a green fluorescent filter. Semi-
228 quantitative analysis was performed using ImageJ software (n=10). In parallel with these
229 experiments, interference controls were also tested [39].
230
231 **2.3.3.3. Thermogravimetric analysis of zebrafish**

232 To determine the accumulation of nanosized zeolite beta during the zebrafish embryonic
233 development, samples were studied by TG analysis. After the estimation of previously
234 mentioned endpoints at 72 hpf, the remaining larvae were rinsed three times with deionized
235 water. Further, fish were sonicated for 2 min, rinsed three times with deionized water, sonicated
236 for an additional 2 min and finally rinsed three times with deionized water. Sonication was
237 conducted twice in order to remove particles that potentially remained at the surface of the fish
238 body. Samples were then incubated at 60°C until a constant dry mass was recorded. Controls

on AW were run in parallel. Considering larvae low body mass, all dried fish per tested sample were transferred into an alumina crucible and heated till 800°C using a Setaram Setsys TGA instrument, heating rate 5°C min^{-1} in air.

2.3.4. Docking

AutoDock Vina [40] version 1.1.2 was used to explore potential binding sites for TEA (tetraethylammonium) cation on the zebrafish hatching enzyme ZHE1 whose structure was taken from the PDB data bank (PDB ID 3LQB) [41]. Atomic coordinates for TEA were also taken from the PDB (PDB ID 1A9X) [42]. Water molecules and cocrystal ligands (sulfate ion, 1,2-ethanediol) were removed from the crystal structure of the hatching enzyme ZHE1, hydrogen and partial Gasteiger charges were added and the coordinates of the structure were saved in pdbqt format. TEA was also converted to a pdbqt file. SwissDock [43] was also used to dock TEA to ZHE1. SwissDock is based on the docking software EADock DSS and the calculations are performed using the CHARMM22/27 all-hydrogen force field [44]. The default parameters were used whereas the whole protein structure was considered as a target during docking.

2.3.4.1. Molecular dynamics simulation

Three different complexes of ZHE1 + TEA were prepared according to three poses obtained by both docking simulations. TEA is described by the general Amber force field (GAFF) [45] with partial charges obtained through the standard restrained electrostatic potentials (RESP) calculations [46] at the HF/6-31G* level of theory with the Gaussian09 simulation package [47]. Hatching enzyme ZHE1 was described with the Amber14SB force field. All complexes were solvated in truncated octahedral boxes of TIP3P water molecules, extending 10 Å from the protein with chloride anions added to neutralize the system. Minimization was conducted in three cycles by restraining different atoms with a force constant of 50 kcal mol^{-1} $Å^{-1}$. In the first cycle, restraint was applied on each protein atom while water, ions, and the substrate were allowed to move by using 500 steps of steepest descent minimization, followed by 1,000 steps of conjugate gradient minimization. In the second cycle, the whole substrates and the protein were fixed using restraint on backbone atoms only, while side chains of the protein, water, and ions were allowed to move using 500 steps of steepest descent, followed by 2,000 steps of conjugate gradient minimization. In the last cycle, the whole system was subjected to 5,000 steps of minimization by applying 1,500 steps of steepest descent and 3,500 steps of conjugate gradient minimization with no applied constraints. Optimized systems were gradually heated

from 0 to 300 K and equilibrated during 50 ps using NVT conditions [constant number (N), volume (V), and temperature (T)]. The density of the system was then equilibrated during 150 ps of the simulation under the NPT ensemble. The system was further equilibrated for 50 ps of the simulation and subjected to productive, unrestrained production simulations in NVT ensample. Bonds involving hydrogen atoms were constrained using the SHAKE algorithm [48]. The time step was 2 fs. The Particle Mesh Ewald method [49] was applied to calculate long-range electrostatic interactions. Nonbonded interactions were truncated at 10.0 Å. The 100 ns production runs were performed on the graphics processing unit (GPU; GeForce GTX 1080Ti) by using the pmemd.CUDA engine [50,51] of AMBER16 [52]. Simulations for each complex were conducted in triplicates resulting in 300 ns of simulations for each complex.

2.5. Statistics

All analysis was conducted using GraphPad Prism 6.01. (GraphPad Software Inc., USA). Statistical differences between nano-zeolite samples/TEOH and negative control (AW) , as well as among nano-zeolite samples and TEAOH treatment group were evaluated by one-way analysis of variance (ANOVA) with Tukey's post hoc test. The results were expressed as means ± SD, and $p \leq 0.05$ was used as a cutoff value of statistical significance. The results of the hatching rate were presented as box-plots. A line within the box represents the median value, while the boundaries of box-plot indicate 25^{th} and 75^{th} percentiles. Whiskers above and below the box indicate 10^{th} and 90^{th} percentiles.

3. Results and discussion

3.1. Physico-chemical characterization of the tested samples

The X-ray powder diffraction patterns (XRD) of two calcined samples are displayed in Fig. 1A. Both XRD patterns of the samples are typical of zeolite beta exhibiting broad peaks arising from the superposition of two systems of broadened reflections associated with polymorphs A and B of zeolite beta. TG analysis of the as-prepared zeolite beta samples was employed to measure the TEAOH content within the zeolite framework (Fig. 1B). Both samples exhibit four weight-loss steps. Two dehydration steps are ranged from room temperature to 180°C and events associated with TEA species release and degradation from 180 to 600°C. Consequently, the content of TEA species in the samples can be calculated from the TG curves. In the sample BEA-140, there is 20 wt% of organic structure-directing agent, while in the BEA-600 the

amount is 17 wt%. The average value of 18 wt% of organic species was taken for embryotoxicity tests.

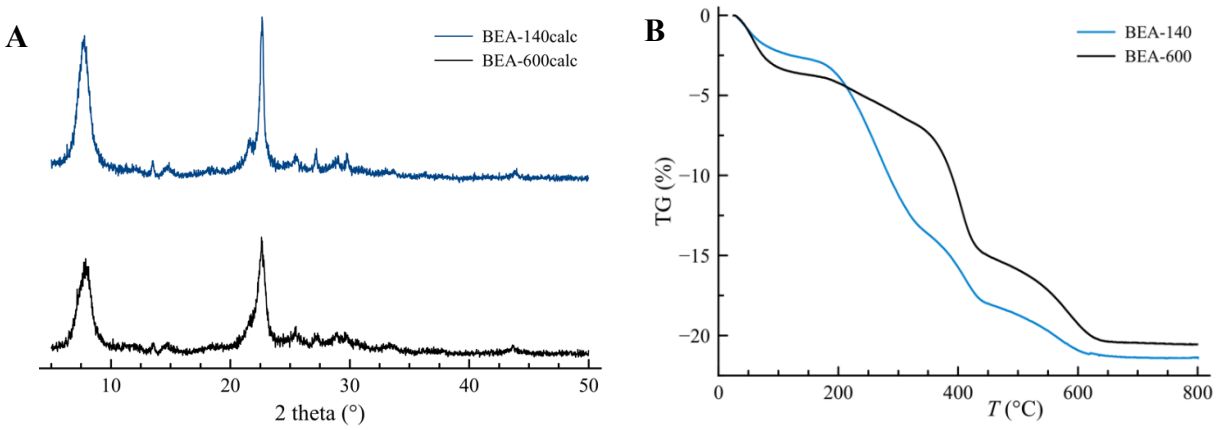

Figure 1. XRD patterns (A) of the calcined nano-zeolite beta samples used in this study and TG curves (B) of the as-prepared nano-zeolite beta samples.

Dynamic light scattering (DLS) measurements of all of the samples were performed using a concentration of 100 µg mL^{-1}, dispersed both in deionized water and in AW. No difference in the size distribution has been observed with respect to the dispersant. Furthermore, for the sake of comparison, two samples having a concentration of 25 µg mL^{-1} dispersed in AW were measured as well (Fig. 2). The maximum position of the DLS size distribution curve of the as-prepared BEA-140 having the concentration 100 µg mL^{-1} is at 140 nm, whereas for the calcined BEA-140-calc (100 µg mL^{-1}) and BEA-140 (25 µg mL^{-1}) the maximum is at 160 nm. In the case of samples BEA-600 and BEA-600-calc (100 µg mL^{-1}), the maximum is achieved at the hydrodynamic diameter of 600 nm. The sample BEA-600 (25 µg mL^{-1}) exhibits a maximum at 520 nm. Thus, considering the observed maximums in the DLS curves, the samples were labeled BEA-140 and BEA-600. The observed minor differences in the positions of the maximum of DLS curves in the studied samples can be attributed to slight fluctuations during the measurement due to the presence of different cations in the dispersant. Still, based on DLS data, it is evident that there is no irreversible aggregation of the zeolite beta particles during the calcination, as was observed previously [53].

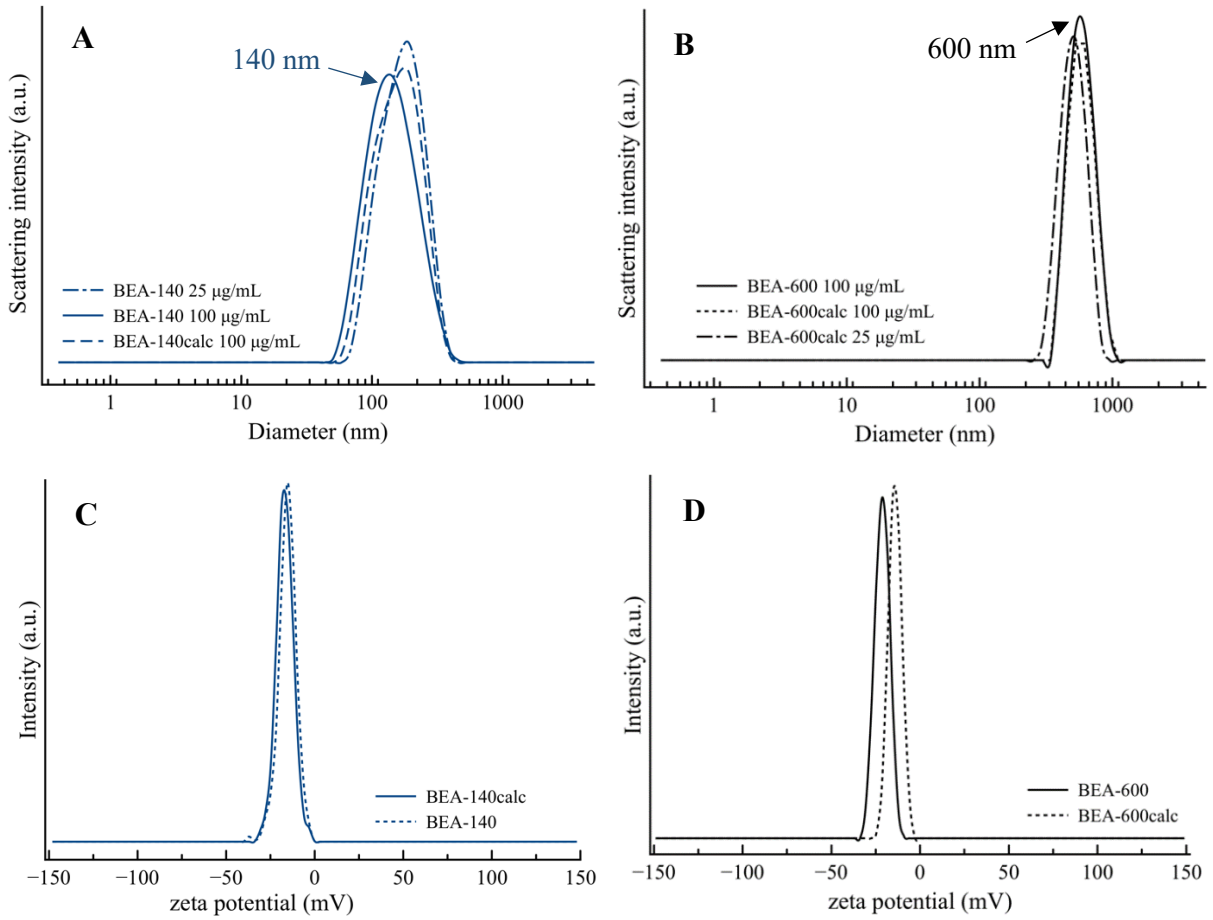

Figure 2. DLS size distribution curves of the studied samples BEA-140 and BEA-600 of different concentrations (A and B) and the zeta potential curves of the nano-zeolite beta suspensions having the concentration 100 µg mL^{-1} (C and D).

Zeta potential measurements provide information on the colloidal stability of the samples. The peaks of the highest studied concentration are positioned at -15.6 mV and at -21.3 mV for the samples BEA-140 and BEA-600, respectively (Fig. 2). The suspensions of pristine samples have more negative zeta potential than the calcined samples – the zeta potential maximum is at -13.7 mV for BEA-140-calc and -12.9 mV for BEA-600-calc. This is expected because of the changing and condensing of the surface silanols of the zeolite beta particles during calcination. In summary, all zeolite samples exhibit a negative zeta potential that prevents particle aggregation but may have an impact on the interactions between the zeolite beta particles and zebrafish.

SEM micrographs (Fig. 3, top) of the zeolite beta samples show that particles are uniform in size and shape in both cases. Crystals in the sample BEA-140 are about 150 nm in size. The particles are rounded and do not have well-defined edges. The crystals in the sample BEA-600 are oval in shape. Their size is around 600 nm. The TEM study (Fig. 3, down) confirms the

uniformity of the zeolite beta particle size and the morphological features observed by SEM. The average size of the particles is about 150 nm and 650 nm in the samples BEA-140 and BEA-600, respectively. In the sample BEA-140, the particles are isometric, while in the BEA-600 they are egg-like/ellipsoids. Thus, the micrographs of the tested samples corroborate the DLS findings.

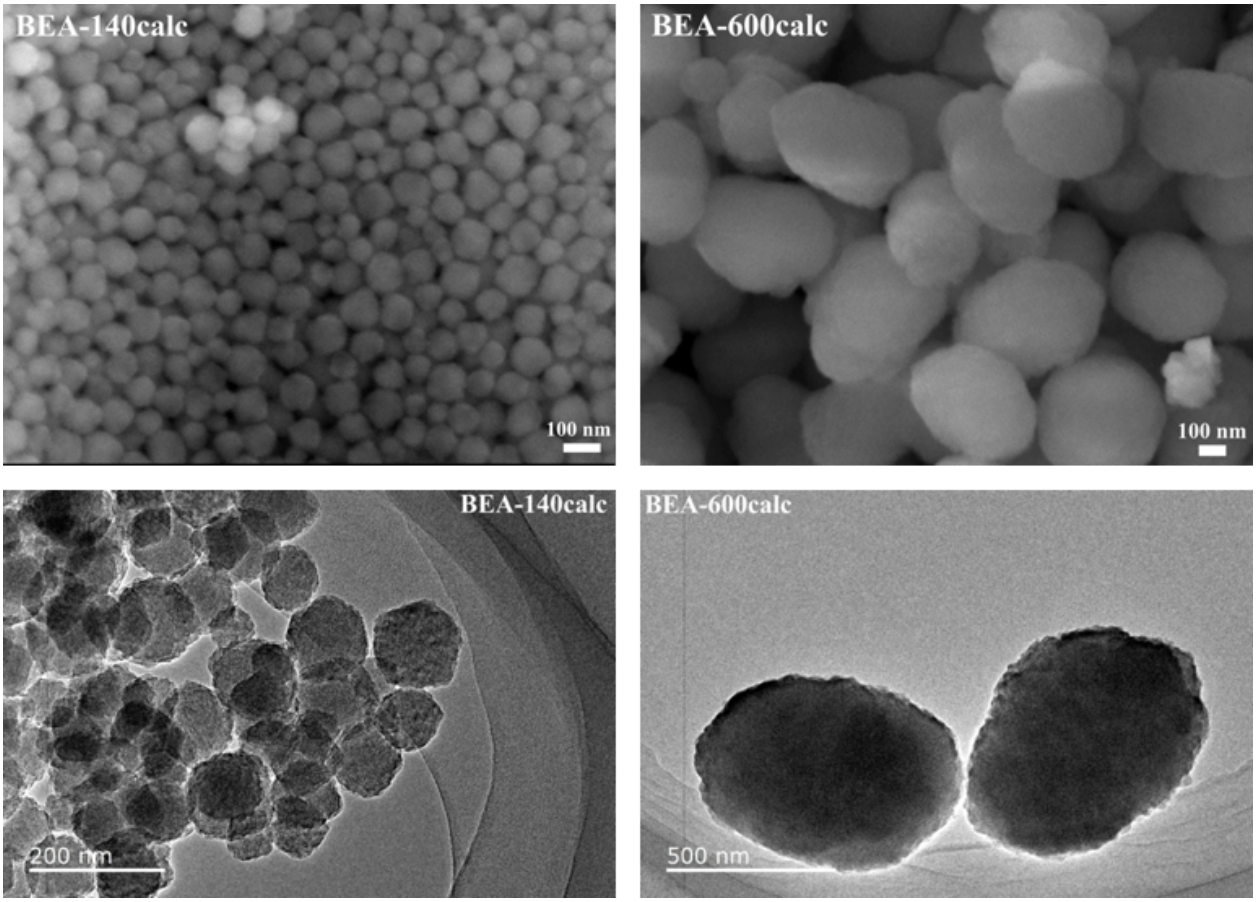

Figure 3. SEM (the first row) and TEM (the second row) images of the studied calcined zeolite beta samples BEA-140calc and BEA-600calc.

3.2. Embryotoxicity test

During 24, 48 and 72 h of zebrafish embryo exposure to the calcined and non-calcined zeolite beta suspensions and TEAOH, only a minor mortality rates (≤7%) were observed (Tbl. 1). Sub-lethal effects on all tested samples (<8%, Tbl. 1) revealed whether through yolk sac edema (Fig. S1, b) or blood accumulation at the yolk sac (Fig. S1, d). Based on the number of survived zebrafish, it can be asserted that all tested samples showed no toxicity or very low acute toxicity with small variances in the percentage of dead and/or abnormal embryos.

Table 1. Overview of endpoints measured at 72 h after *D. rerio* embryos exposure to the tested samples.

			Observed endpoint			
		Dose (μg mL^{-1})	**Lethal embryos (%)**	**Affected embryos (%)**	**Heart beat rate (beats/15 sec)**	**Pigmentation formation (scored 1-3)**
Control	**Artificial water**	**-**	0.00 ± 0.00	3.33 ± 5.77	39.71 ± 1.25	2.93 ± 0.25
Zeolites	**BEA-140-calc**	**25**	0.00 ± 0.00	0.00 ± 0.00	38.88 ± 1.96	2.90 ± 0.31
		50	0.00 ± 0.00	0.00 ± 0.00	37.81 ± 1.83	2.90 ± 0.31
		100	0.00 ± 0.00	3.33 ± 5.77	36.38 ± 1.50	2.93 ± 0.25
	BEA-600-calc	**25**	0.00 ± 0.00	0.00 ± 0.00	37.44 ± 1.59	2.96 ± 0.18
		50	0.00 ± 0.00	3.33 ± 5.77	39.57 ± 1.90	2.90 ± 0.31
		100	6.66 ± 5.77	3.57 ± 5.77	35.00 ± 1.41	2.90 ± 0.31
Zeolites with OSDA	**BEA-140**	**25**	0.00 ± 0.00	0.00 ± 0.00	38.02 ± 1.92	2.93 ± 0.25
		50	3.33 ± 5.77	3.83 ± 6.41	38.40 ± 3.13	2.96 ± 0.18
		100	3.33 ± 5.77	3.34 ± 5.77	38.42 ± 1.13	2.90 ± 0.31
	BEA-600	**25**	0.00 ± 0.00	3.33 ± 5.77	38.20 ± 1.90	2.96 ± 0.18
		50	0.00 ± 0.00	3.33 ± 5.77	38.88 ± 0.83	2.93 ± 0.25
		100	6.66 ± 5.77	3.97 ± 6.41	41.63 ± 1.19	2.90 ± 0.31
OSDA	**TEAOH**	**4.5**	0.00 ± 0.00	0.00 ± 0.00	48.14 ± 1.68***	2.93 ± 0.25
		9	6.66 ± 5.77	3.97 ± 6.41	46.71 ± 1.80***	2.90 ± 0.31
		18	6.66 ± 5.77	7.54 ± 6.11	42.33 ± 1.50*	2.90 ± 0.31

*p<0.05, ***p<0.0001

As previously reported [7], nanoparticles with high positive zeta potential values are usually cytotoxic, while neutral and negatively charged nanoparticles have no negative impact on the cell. To support this theory Georgieva et al. [7] reported no impact of zeolite EMT nanoparticles on human glioblastoma U87-MG and human kidney HEK-293T cell lines viability due to exposure to negatively charged zeolite nanoparticles (10-30 nm; 50-400 μg mL^{-1}). Moreover, Laurent et al. [17] showed that the viability of human cervical adenocarcinoma (HeLa) cells was also not significantly affected after interaction with ultra-small LTL and EMT zeolites (8–18 nm) free of organic templates (50-400 μg mL^{-1}). Based on the number of survived zebrafish, it can be asserted that all tested samples showed no toxicity or very low acute toxicity with small variances in the percentage of dead and/or abnormal embryos/larvae.

Since there is a possibility of the TEA leaching from the zeolite channels, which may have an impact on the results obtained for the pristine nano-sized zeolite beta sample, the toxicity of TEA alone was tested as well. Upon exposure to 4.5, 9 and 18 µg mL^{-1} TEAOH (corresponding to the TEA concentrations present in 25, 50 and 100 µg mL^{-1} of non-calcined BEA-140 and BEA-600 samples, respectively) heart rate significantly increased (Tbl. 1, marked gray), which was not manifested in accelerated movements. According to the results obtained during exposure to BEA-140 and BEA-600, nano-sized zeolite beta samples prevented the cardiotoxic effect of the TEA. Still, avoiding the presence of organic structure-directing agents is indispensable for further practical uses of nanosized zeolites, especially for biomedical applications. This claim has been pointed up by further observation of larvae hatching. Hatching is a critical stage in zebrafish life since it represents the end of embryogenesis and the start of their swimming life phase. Decreased hatching success can increase predation or lead to fish death within the chorion. Moreover, hatching disruption can cause a negative impact at the population level, affecting thus ecosystems [55]. Calcined zeolite nanoparticles tested within this study did not affect zebrafish hatching, while on the other hand, strong inhibition of hatching rate at 72 hpf was recorded on non-calcined BEA-140 and BEA-600 samples (Fig. 4). The highest concentration of the sample BEA-140 caused the largest hatching rate reduction at 72 hpf (96.55% compared to the control values; Fig. 4). TEA caused also a statistically significant decrease of hatching rate, but those values were lower (~65% of zebrafish hatched during a 72-h exposure to 18 µg mL^{-1} of TEAOH).

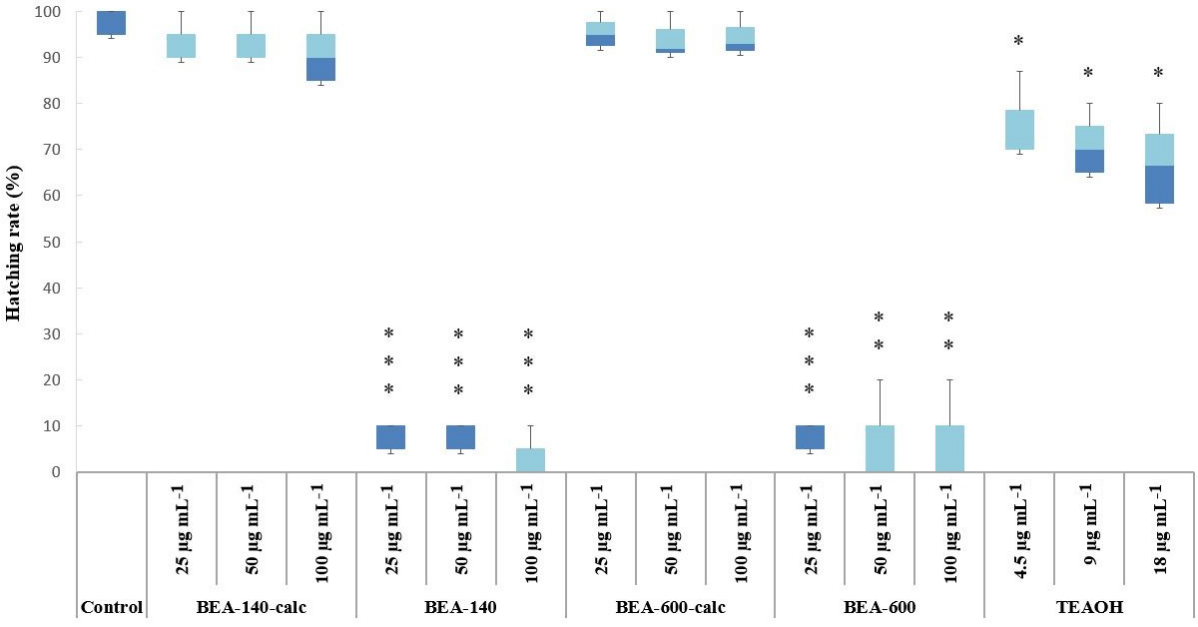

Figure 4. Hatching rate of 72 h old *D. rerio* embryos after exposure to the nano-zeolite beta suspensions and TEAOH. Statistical differences relative to the control group: *p<0.05, **p<0.001, ***p<0.0001.

It is important to note that treated fish were not morphologically different from control fish, indicating that delayed hatching was not caused by slowed morphological development and thus by slowed maturation of the hatching gland. Since this option seems unfeasible, we investigated other possible mechanisms of the observed hatching inhibition. Hatching in zebrafish is regulated by exogenous factors such as light-dark cycles, oxygen levels, etc., but also endogenous factors such as muscle contractions, hormonal levels, the release of proteolytic enzymes from specialized cells [55]. Since the experiment was conducted in controlled conditions (light, temperature, oxygen level), the reason for decreased hatching was searched among endogenous factors. De la Paz et al. [55] reported that zebrafish hatching enzyme (ZHE1) expressed in the hatching gland is responsible for chorion degradation allowing zebrafish to hatch. Therefore, the inhibition of enzyme ZHE1 could lead to hatching retardation. Previous studies have shown that EDTA [56] and triazoles [55] inhibit hatching through affecting the hatching enzyme, either by complexing its Zn^{2+} ion or impairing the release of ZHE1 enzyme, respectively. To probe whether TEA directly binds to ZHE1 enzyme and interferes with the hatching process we performed docking simulations using two different docking programs AutoDock Vina and SwissDock. Molecular dynamics simulations were used to probe how specific are binding sites and poses found by docking simulations. Only those binding positions, found by both programs, were analyzed. Consequently, three different binding sites were identified (Fig. 5). Within the binding site *a*, TEA and Tyr93 interact through cation-π interactions; Asp34 interacts with the TEA through electrostatic interactions, whereas ethyl groups of the TEA interact with Val37 and Val92 through van der Waals interactions. Within the binding site *b*, the TEA is bound within the enzyme active site. Cation-π interactions are established between TEA and Tyr155 and Phe160, whereas Ile98 makes van der Waals interactions with ethyl groups of TEA. Glu100 makes electrostatic interactions with cationic TEA. Within the binding site *c*, cation-π interactions are established between TEA and Trp12, electrostatic interactions are established with Glu21 and Asp61, whereas TEA makes hydrophobic interactions with Pro23.

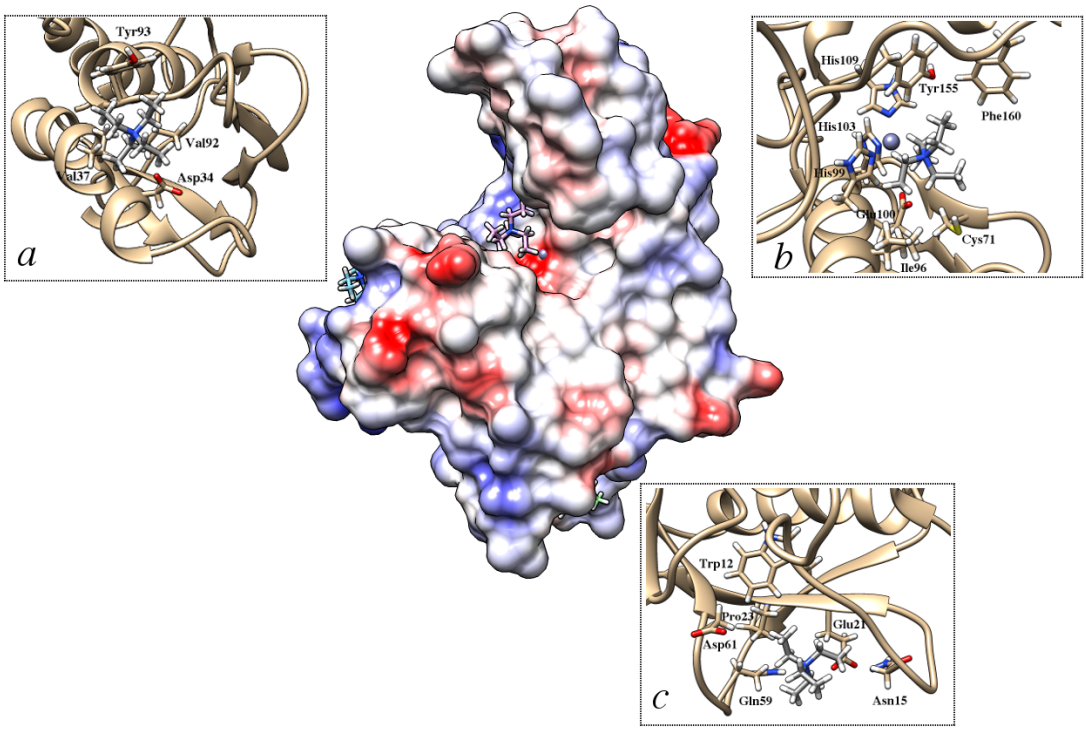

Figure 5. Three binding sites *a*, *b* and *c* obtained using AutoDock Vina and SwissDock docking software. Protein surface is colored according to electrostatic potential, where red stands for negative, white for neutral and blue for positive potential. TEA is shown in grey.

To probe how specific these interactions are, we simulated three complexes for molecular-dynamics simulations according to binding poses obtained using AutoDock Vina and SwissDock (Fig. 5). Each complex was simulated in three independent replicas according to the protocol described in Materials and methods. Our unconstrained simulations have shown that binding of TEA is nonspecific. What was common for all three complexes is that after 20 ns of simulations TEA dissociated from ZHE1 into bulk water. The simulations were repeated with all ligand atoms restrained by the harmonic potential with the force constant of 100 kcal mol^{-1} $Å^{-1}$ during optimization, equilibration and first 20 ns of MD simulation, after which force constant was gradually decreased. This was then followed by unconstrained MD simulations. However, in all three cases, TEA dissociated from the ZHE1 enzyme into bulk water again, definitely referring to nonspecific binding of TEA to the ZHE1 enzyme. *In silico* study implies that TEA does not bind to the ZHE1 enzyme which therefore excludes the inhibition of the ZHE1 enzyme as a possible mechanism of hatching retardation.

It has been previously shown that tetraalkylammonium salts are reversible inhibitors of cholinesterases [57], which was our rationale behind investigating whether TEA binds to and inhibits ZHE1 enzyme. Another study has shown that organic cations, such as

tetramethylammonium (TMA) and TEA, can replace Mg^{2+} and Ca^{2+} ions in bacteriorhodopsin and maintain proton pumping ability [58]. In our case, displacement of Zn^{2+} ions with organic cation would inhibit the enzyme and consequently, the hatching process, because zebrafish hatching enzyme 1 is a Zn-protease needing Zn^{2+} as a catalytically active cation. This is in line with the previous study that demonstrated complete loss of enzyme activity in the presence of a chelating agent EDTA [56]. It has also been demonstrated that 4 metal oxide nanoparticles (CuO, ZnO, Cr_2O_3, and NiO) interfere with zebrafish hatching by shedding metal ions which then ligate to critical histidines in the ZHE1 active site [59]. In another study, the addition of the metal ion chelator, diethylene triamine pentaacetic acid (DTPA), reversed the hatching interference of the shed Cu^{2+}, Zn^{2+}, and Ni^{2+} cations, proving that inhibition is indeed due to the shedding of metal ions [60]. Moreover, studies conducted on related zinc metalloprotease showed that substituting Zn^{2+} with Cu^{2+} or Ni^{2+} results in reduced or diminished enzyme activity [61,62]. Therefore, to investigate whether TEA could replace Zn^{2+} and stay stably bound, which would result in an inactive enzyme, we have additionally prepared another complex of ZHE1 with TEA, in which the organic cation occupies Zn^{2+} binding site. However, our three independent MD simulations showed that TEA dissociates from the enzyme into bulk water within the first 15 ns of MD simulations. Thus, TEA does not inhibit the enzyme by displacing the Zn^{2+} cation.

3.3. ROS and apoptosis detection

Generation of ROS and apoptosis are normal parts of the development and essential for normal cellular functioning. Despite, homeostatic cellular balance can be disrupted by exposure to e.g. toxicants, consequently resulting in ROS overproduction and cell death. Zebrafish exposure to pristine BEA-140 and BEA-600 samples, as well as TEAOH, resulted in a significant increase of the mean green fluorescence intensity (Fig. 6). Contrary, DCF and AO staining showed no significant ROS and/or apoptosis formation during exposure to calcined zeolite samples (Fig. 6, b). The highest increase of ROS production in larvae exposed to BEA-600 and BEA-140, followed by TEAOH (4.21, 3.24 and 2.30 times increased compared to the control, respectively). Moreover, fish treated with BEA-140 and BEA-600 samples and stained with AO showed green fluorescent apoptotic spots on the heart, eye and head region (Fig. 6, a). Such finding was also observed during exposure to TEAOH. The results confirmed the dependence of cellular apoptosis with ROS induction in the whole zebrafish larvae, as is already recorded by Kumar et al. [63].

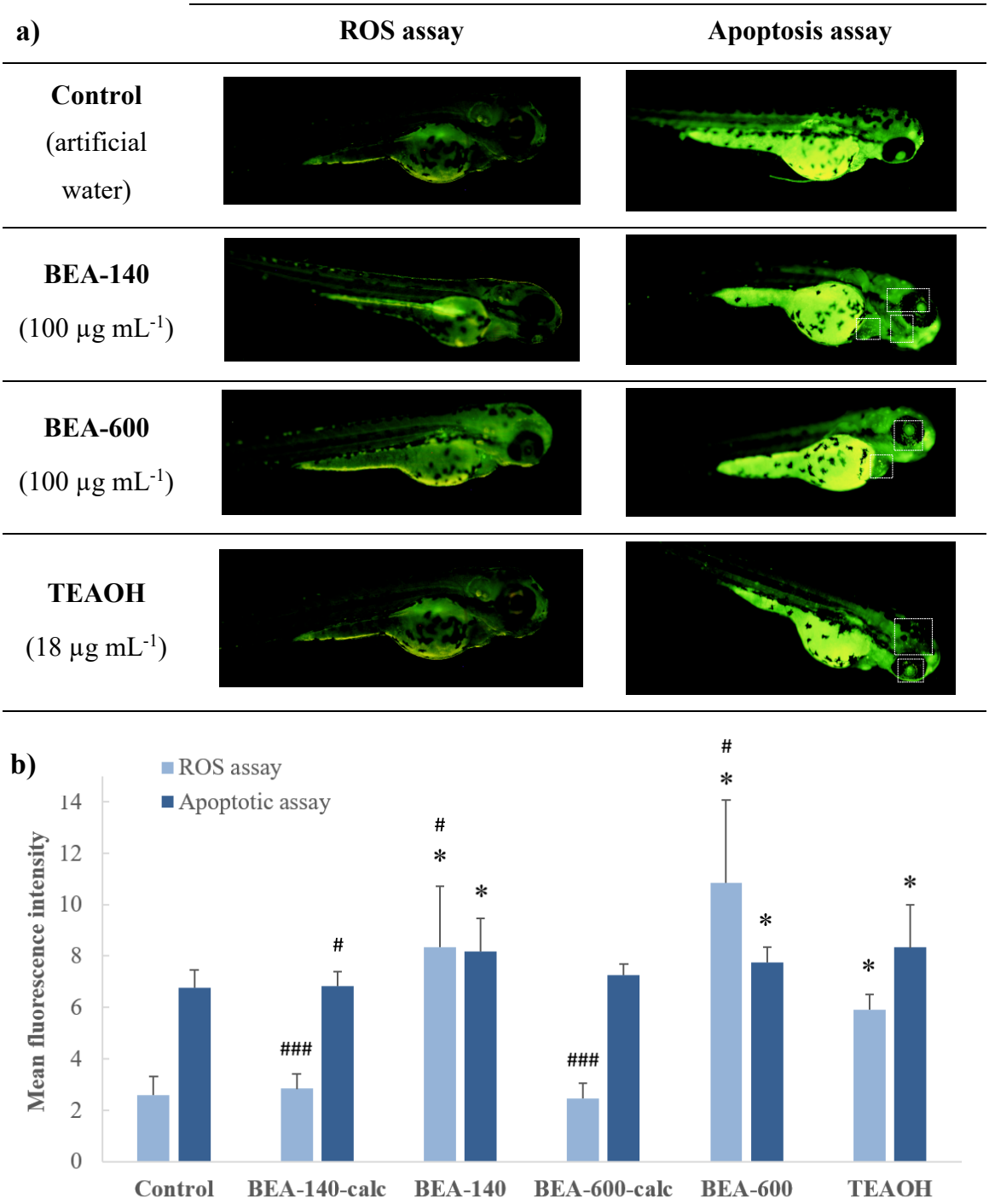

Figure 6. (a) Fluorescent images of *D. rerio* larvae stained with ROS marker DCF and apoptosis marker AO after 72 h of exposure to tested nano-zeolite beta suspensions and TEAOH. (b) The bar graph represents the mean fluorescent intensity of DCF and AO in the whole larvae. The AO positive cells were indicated by dashed rectangles. Fluorescent intensity was calculated using Image J and the values were presented as the mean of fluorescence intensity ± SD.

Statistical differences from the fluorescent intensity of untreated control larvae: *p<0.05, and from the fluorescent intensity of TEAOH treatment group: #p<0.05, ###p<0.05.

The absence of negative impact of calcined samples was in line with the study of Laurent et al. [17] which although confirmed internalization of ultra-small zeolites in HeLa cells, recorded neither oxidative stress nor abnormality in DNA replication. Considering the results obtained on non-calcined samples and TEAOH, we can conclude that OSDA leached to a certain extent from the zeolite, thus leading to ROS formation. To date, several authors emphasized that oxidative stress caused by ROS could lead to hatching delay [64,65]. For that reason, we propose that exactly oxidative stress is the major mechanism underlying the toxicity of non-calcined samples and TEAOH recorded within this study. Moreover, it is important to note that the TEA itself caused a significantly lower increase of the mean green fluorescence intensity (oxidative stress) than the as-prepared zeolite samples ($p<0.05$; Fig. 6). Regarding conducted interference controls, we did not observe any fluorescence, proving that nano-zeolite samples did not produce fluorescence that would lead to false-positive results.

In addition, microscopic pictures of the chorion (magnification 100x) were taken (Fig. S2). As can be seen, zeolite samples agglomerated at the surface of the zebrafish chorion. Considering that, if OSDA leaching occurred at the surface of the chorion, fish would be in direct and constant exposure, thus displaying higher oxidative stress than recorded during exposure to TEAOH itself.

Such observation of nanoparticle aggregation is not uncommon. Kashiwada [66] investigated the distribution of water-suspended fluorescent nanoparticles (solid latex solution) in the eggs and shown that nanoparticles in the range from 39.4 to 42.0 nm in diameter also aggregate and adsorb on the chorion of medaka eggs. Such aggregation at the surface of the chorion can negatively affect the nutrient absorption but also vitamin synthesis [67], impacting thus zebrafish embryonic development. Accordingly, limitations of chorion permeability for nanoparticles, as well as nanoparticle aggregation and adsorption on the chorion should be taken into account during the toxicity evaluation of nanoparticles on zebrafish embryos.

3.4. TG analysis – interactions between zebrafish and zeolite nanoparticles

Many studies emphasize the fact that the chorion represents a barrier of limited permeability, highlighting thus their importance during embryonic development of zebrafish [68,69]. The pore size of the chorion is estimated from 0.6 - 0.7 μm [69], which is in theory larger than the size of zeolite nanoparticles used within this study. Despite nanoparticles are known to

aggregate and form larger agglomerates which complicate their interaction with the model organism Kim and Tanguay [69] and Kashiwada [66] pointed out that such observation did not prevent their accumulation in medaka fish. In fact, 474-nm water-suspended fluorescent nanoparticles had the highest bioavailability to eggs, while particles of 39.4 nm in diameter shifted into the yolk and gallbladder along with embryonic development [66]. To date, it is entirely unknown whether zeolite beta nanoparticles can enter the embryos and whether they are biocompatible. Thus, TG analysis of the dried fish was performed in order to determine if tested zeolite samples interact with the chorion/fish (Tbl. 2). The weight fraction of the solid residue for the control was 7.03 wt% of the initial mass of the dried larvae. TG analysis confirmed that the larvae which were exposed to zeolite beta suspensions exhibit a higher quantity of the solid phase remaining after the analysis, but differences are observed according to the particle size.

Considering the results of TG analysis and the fact that fish exposed to BEA-140-calc hatched normally, while specimens exposed to BEA-140 stayed within the chorion at 72 hpf (Fig. S2), we speculate that the crystals of BEA-140-calc and BEA-140 (particle size 140 nm) passed through the chorion and accumulated inside the model organism. The value of the difference obtained by TG analysis between the BEA-140-calc and BEA-140 represents the amount of the zeolite beta sample that was bonded to/accumulated in larvae (+4.19 and +4.86 wt%, respectively) (Tbl. 2). Further research is needed to confirm this interaction and accumulation of nanosized zeolites in/on the hatched larvae. The increase of the mass of the solid residue after TG measurement for the samples BEA-600-calc and BEA-600 is lower than for the samples comprising smaller particles, +2.94 and + 3.38 wt%, respectively (Tbl. 2), yet still notable. The collected data strongly suggest not only that zeolite beta particles have strong interaction with the chorion and subsequently with the embryos, but also that they remained firmly bonded even after several cycles of ultrasonication.

Table 2. TG analysis of the washed and dried *D. rerio* larvae exposed to nanosized zeolite beta suspensions for 72 h.

Sample	**Fraction of the solid residue**	**Difference to control**
Control	7.03 wt%	-
BEA-140	11.89 wt%	+4.86 wt%
BEA-140calc	11.22 wt%	+4.19 wt%
BEA-600	9.97 wt%	+2.94 wt%
BEA-600calc	10.41 wt%	+3.38 wt%

4. Conclusion

Stable suspensions of pristine and calcined zeolite beta nanoparticles (140 and 600 nm) in AW have been prepared and their potential toxicity towards zebrafish *Danio rerio* embryos was evaluated. The results indicate that non-calcined beta zeolites containing TEA caused zebrafish hatching inhibition accompanied by oxidative stress. A similar effect was observed with TEAOH. The assumption that the observed effects are due to the TEA interactions with the zebrafish hatching enzyme ZHE1 has been validated by molecular docking and molecular dynamics simulations. However, the computational investigation points out that the TEA does not bind to the ZHE1 enzyme thus excluding the ZHE1 enzyme inhibition as a potential cause of the hatching reduction. Hence, the observed hatching delay of the non-calcined zeolite suspensions and TEAOH was, as detected using fluorescence microscopy, attributed to the oxidative stress. This is further supported by the finding that the zebrafish embryos developed normally in the presence of the calcined zeolite nanoparticles despite the strong interaction with the chorion and subsequently with the embryos. In addition, the necessity to decrease the quantity of the organic structure-directing agents in zeolite synthesis reaction mixtures was shown. Finally, the obtained results have shown that selected model organisms could improve our ability to understand the mechanism of the toxicity of alumosilicates, and should be incorporated in nanoparticle toxicity monitoring and risk assessment studies in materials science in general.

Declaration of competing interest

All authors have no potential sources of conflict of interest.

Acknowledgments

The financial support from the Croatian Academy of Science and experiment.com platform is gratefully acknowledged. This study was partially supported by the Scientific Centre of Excellence for Marine Bioprospecting – BioProCro, a project co-financed by the Croatian Government and the European Union through the European Regional Development Fund - the Competitiveness and Cohesion Operational Programme (KK.01.1.1.01). A.M. would like to thank the Zagreb University Computing Centre (SRCE) for granting computational resources on the ISABELLA cluster.

References

[1] V. Valtchev, L. Tosheva, Chem. Rev. 113 (2013) 6734-6760. https://doi.org/10.1021/cr300439k

[2] http://www.hypotheticalzeolites.net (accessed January 31, 2020)

[3] http://www.iza-structure.org/databases (accessed January 31, 2020)

[4] G. Bellussi, R. Millini, P. Pollesel, C. Perego, New J. Chem. 40 (2016) 4061-4077. https://doi.org/10.1039/c5nj03498a

[5] S.E. Lehman, S.C. Larsen, Environ. Sci.: Nano 1 (2014) 200-213. https://doi.org/10.1039/c4en00031e

[6] S. Mintova, M. Jaber, V. Valtchev, Chem. Soc. Rev. 44 (2015) 7207-7233. https://doi.org/10.1039/c5cs00210a

[7] V. Georgieva, C. Anfray, R. Retoux, V. Valtchev, S. Valable, S. Mintova, Micropor. Mesopor. Mater. 232 (2016) 256-263. https://doi.org/10.1016/j.micromeso.2016.06.015

[8] M. Koehle, R.F. Lobo, Catal. Sci. Technol. 6 (2016) 3018-3026. https://doi.org/10.1039/c5cy01501d

[9] W.J. Roth, P. Nachtigall, R.E. Morris, J. Čejka, Chem. Rev. 114 (2014) 4807-4837. https://doi.org/10.1021/cr400600f

[10] H.Y. Luo, J.D. Lewis, Y. Román-Leshkov, Annu. Rev. Chem. Biomol. Eng. 7 (2016) 663-92. https://doi.org/10.1146/annurev-chembioeng-080615-034551

[11] H. Awala, J.P. Gilson, R. Retoux, P. Boullay, J.M. Goupil, V. Valtchev, S. Mintova, Nature Mater. 14 (2015) 447-451. https://doi.org/10.1038/nmat4173

[12] L. Kyu, L.B., Huong, P.T., Geun LD. Kyu, Method for Removing Carbon Dioxide Using Nano-Zeolite Supported with Fe Ion., (2016) Pat. KR20170142691.

[13] M. Nishihara, Y. Terayama, T. Haji, S.M. Lyth, S. Satokawa, H. Matsumoto, eXPRESS Polymer Lett. 12, (2018) 256-264. https://doi.org/10.3144/expresspolymlett.2018.23

[14] Q. Li, G. Liao, S. Zhang, L. Pang, H. Tong, W. Zhao, Z. Xu, Appl. Surf. Sci. 427 (2018) 437-450. https://doi.org/10.1016/j.apsusc.2017.08.024

[15] G.S. Wang J, Zhang J, Triethylamine Fluorescence Sensor for Detecting e.g. Triethylamine Gas, Comprises Nano-L-Type Zeolite and Rare-Earth Beta-Diketone Complex Obtained by Reacting Rare-Earth Ion and β-Diketone Ligand., (2017) Pat. CN107089905-A.

[16] C.R. Thomas, S. George, A.M. Horst, Z. Ji, R.J. Miller, J.R. Peralta-Videa, T. Xia, S. Pokhrel, L. Mädler, J.L. Gardea-Torresdey, P.A. Holden, A.A. Keller, H.S. Lenihan, A.E. Nel, J.I. Zink, ACS Nano 5 (2011) 13-20. https://doi.org/10.1021/nn1034857

[17] S. Laurent, E.P. Ng, C. Thirifays, L. Lakiss, G.M. Goupil, S. Mintova, C. Burtea, E. Oveisi, C. Hébert, M. De Vries, M.M. Motazacker, F. Rezaee, M. Mahmoudi, Toxicol. Res. 2 (2013) 270-279. https://doi.org/10.1039/c3tx50023c

[18] L.C.J. Thomassen, D. Napierska, D. Dinsdale, N. Lievens, J. Jammaer, D. Lison, C.E.A. Kirschhock, P.H. Hoet, J.A. Martens, Nanotoxicology 6 (2012) 472-485. https://doi.org/10.3109/17435390.2011.587901

[19] P.D. Noyes, G.R. Garcia, R.L. Tanguay, Green Chem. 18 (2016) 6410-6430. https://doi.org/10.1039/c6gc02061e

[20] D.H. Pham, B. De Roo, X.B. Nguyen, M. Vervaele, A. Kecskés, A. Ny, D. Copmans, H. Vriens, J.P. Locquet, P. Hoet, P.A.M. De Witte, Sci. Rep. 6 (2016) 37145. https://doi.org/10.1038/srep37145

[21] A.P. Deveau, V.L. Bentley, J.N. Berman, 45, (2017) 1-9. https://doi.org/10.1016/j.exphem.2016.09.012

[22] D.D. Nabinger, S. Altenhofen, P.E.R. Bitencourt, L.R. Nery, C.E. Leite, M.R.M.R. Vianna, C.D. Bonan, Sci Total Environ. 624 (2018) 1623-1633. https://doi.org/10.1016/j.scitotenv.2017.10.057

[23] D. Bridi, S. Altenhofen, J.B. Gonzalez, G.K. Reolon, C.D. Bonan, Toxicology. 392 (2017) 32-39. https://doi.org/10.1016/j.tox.2017.10.007

[24] H.C Liu, T.Y. Chu, L.L. Chen, W.J. Gui, G.N. Zhu, Environ. Pollut. 231 (2017) 1093-1103. https://doi.org/10.1016/j.envpol.2017.05.072

[25] G. Malafaia, A.M. de Souza, A.C. Pereira, S. Gonçalves, A.P. da Costa Araújo, R.X. Ribeiro, T.L. Rocha, Sci. Total Environ. 700 (2020) 1348673. https://doi.org/10.1016/j.scitotenv.2019.134867

[26] L. Qiang, J. Cheng, Ecotoxicol. Environ. Safety 176 (2019) 226-233. https://doi.org/10.1016/j.ecoenv.2019.03.088

[27] S. Babić, J. Barišić, H. Višić, R. Sauerborn Klobučar, N. Topić Popović, I. Strunjak-Perović, R. Čož-Rakovac, G. Klobučar, Water Research 115 (2017) 9-21. https://doi.org/10.1016/j.watres.2017.02.049

[28] M.A.G. Barbosa, R. Capela, J. Rodolfo, E. Fonseca, R. Montes, A. André, A. Capitão, A.P. Carvalho, J.B. Quintana, L.F.C. Castro, M.M. Santos, Ecotoxicol. Environ. Safety 182 (2019) 1094062. https://doi.org/10.1016/j.ecoenv.2019.109406

[29] L. Wu, Y. Jiang, L. Zhang, L. Chen, H. Zhang, Environ Sci Pollut Res Int. 21 (2014) 2663-2676. https://doi.org/10.1007/s11356-013-2193-9

[30] N.B. Abramenko, T.B. Demidova, E. V. Abkhalimov, B.G. Ershov, E.Y. Krysanov, L.M. Kustov, J. Hazard. Mater. 347 (2018) 89-94. https://doi.org/10.1016/j.jhazmat.2017.12.060

[31] J. Duan, Y. Yu, Y. Li, Y. Li, H. Liu, L. Jing, M. Yang, J. Wang, C. Li, Z. Sun, Nanotoxicology 10 (2016) 575-585. https://doi.org/10.3109/17435390.2015.1102981

[32] M. Ghobadian, M. Nabiuni, K. Parivar, M. Fathi, J. Pazooki, Ecotoxicol. Environ. Safety 122 (2015) 260-267. https://doi.org/10.1016/j.ecoenv.2015.08.009

[33] O. Larlus, V.P. Valtchev, Chem. Mater. 17 (2005) 881-886. https://doi.org/10.1021/cm048799r

[34] M. V. Landau, L. Vradman, V. Valtchev, J. Lezervant, E. Liubich, M. Talianker, Ind. Eng. Chem. Res. 42 (2003) 2773–2782. https://doi.org/10.1021/ie020899o

[35] M.A. Camblor, J. Pérez-Pariente, Zeolites 11 (1991) 202-210. https://doi.org/10.1016/S0144-2449(05)80220-9

[36] European Parliament and Council of the European Union, Directive 2010/63/EU of the European Parliament and of the Council of 22 September 2010 on the protection of animals used for scientific purposes, 2013. https://doi.org/doi:10.3000/19770677.L_2013.124.eng

[37] OECD, Test No. 236: Fish Embryo Acute Toxicity (FET) Test., OECD Guidelines for the Testing of Chemicals, Section 2, OECD Publishing. (2013). https://doi.org/10.1787/9789264203709-en

[38] W.S. Lee, H.J. Cho, E. Kim, Y.H. Huh, H.J. Kim, B. Kim, T. Kang, J.S. Lee, J. Jeong, Nanoscale 11 (2019) 3173-3185. https://doi.org/10.1039/c8nr09321k

[39] C. Schimpel, B. Rinner, M. Absenger-Novak, C. Meindl, E. Fröhlich, A. Falk, A. Zimmer, E. Roblegg, E. NanoTox-Lett. 6 (2015) 1-14. https://doi.org/10.1515/entl-2015-0006

[40] O. Trott, A.J. Olson, J. Comput. Chem. 31 (2010) 455-461. https://doi.org/10.1002/jcc.21334

[41] A. Okada, K. Sano, K. Nagata, S. Yasumasu, J. Ohtsuka, A. Yamamura, K. Kubota, I. Iuchi, M. Tanokura, J. Mol. Biol. 402 (2010) 865-878. https://doi.org/10.1016/j.jmb.2010.08.023

[42] J. Wang, R.M. Wolf, J.W. Caldwell, P.A. Kollman, D.A. Case, J. Comput. Chem. 25 (2004) 1157-1174. https://doi.org/10.1002/jcc.20035

[43] A. Grosdidier, V. Zoete, O. Michielin, Nucleic Acids Res. 39 (2011) W270–W277. https://doi.org/10.1093/nar/gkr366

[44] B.R. Brooks, C.L. Brooks, A.D. Mackerell, L. Nilsson, R.J. Petrella, B. Roux, Y. Won, G. Archontis, C. Bartels, S. Boresch, A. Caflisch, L. Caves, Q. Cui, A.R. Dinner, M. Feig, S. Fischer, J. Gao, M. Hodoscek, W. Im, K. Kuczera, T. Lazaridis, J. Ma, V. Ovchinnikov, E. Paci, R.W. Pastor, C.B. Post, J.Z. Pu, M. Schaefer, B. Tidor, R.M. Venable, H.L. Woodcock, X. Wu, W. Yang, D.M. York, M. Karplus, J. Comput. Chem. 30 (2009) 1545-614. https://doi.org/10.1002/jcc.21287

[45] J. Wang, R.M. Wolf, J.W. Caldwell, P.A. Kollman, D.A. Case, J. Comput. Chem. 25 (2004) 1157-1174. https://doi.org/10.1002/jcc.20035

[46] P. Cieplak, W.D. Cornell, C. Bayly, P.A. Kollman, J. Comput. Chem. 16 (1995) 1357-1377. https://doi.org/10.1002/jcc.540161106

[47] M.J. Frisch, G.W. Trucks, H.B. Schlegel, G.E. Scuseria, M.A. Robb, J.R. Cheeseman, et al. Gaussian 09 Revision D.01., Gaussian Inc., Wallingford CT. (2010).

[48] J.P. Ryckaert, G. Ciccotti, H.J.C. Berendsen, J. Comput. Phys. 23 (1977) 327-341. https://doi.org/10.1016/0021-9991(77)90098-5

[49] T. Darden, D. York, L. Pedersen, J. Chem. Phys. 98 (1993) 10089. https://doi.org/10.1063/1.464397

[50] A.W. Götz, M.J. Williamson, D. Xu, D. Poole, S. Le Grand, R.C. Walker, J. Chem. Theory Comput. 8 (2012) 1542-1555. https://doi.org/10.1021/ct200909j

[51] R. Salomon-Ferrer, A.W. Götz, D. Poole, S. Le Grand, R.C. Walker, J. Chem. Theory Comput. 9 (2013) 3878-3888. https://doi.org/10.1021/ct400314y

[52] D. Case, R.M. Betz, D.S. Cerutti, T.E. Cheatham III, T.A. Darden, R.E. Duke, et al., Amber 2016, University of California, San Francisco. (2016).

[53] M. Smaïhi, E. Gavilan, J.O. Durand, V.P. Valtchev, J. Mater. Chem. 14 (2004) 1347-1351. https://doi.org/10.1039/b400521j

[54] S. Laurent, E.P. Ng, C. Thirifays, L. Lakiss, G.M. Goupil, S. Mintova, C. Burtea, E. Oveisi, C. Hébert, M. De Vries, M.M. Motazacker, F. Rezaee, M. Mahmoudi, Toxicol. Res. 2 (2013) 270-279. https://doi.org/10.1039/c3tx50023c

[55] J.F. De La Paz, N. Beiza, S. Paredes-Zúñiga, M.S. Hoare, M.L. Allende, Int. J. Mol. Sci. 18 (2017) 710. https://doi.org/10.3390/ijms18040710

[56] K. Sano, K. Inohaya, M. Kawaguchi, N. Yoshizaki, I. Iuchi, S. Yasumasu, FEBS J. 275 (2008) 5934-5946. https://doi.org/10.1111/j.1742-4658.2008.06722.x

[57] J. Stojan, M. Golicnik, M.T. Froment, F. Estour, P. Masson, Eur. J. Biochem. 269 (2002) 1154-1161. https://doi.org/10.1046/j.1432-1033.2002.02749.x

[58] E.H.L. Tan, D.S.K. Govender, R.R. Birge, J. Am. Chem. Soc. 1996 (1996) 2752-2753. https://doi.org/10.1021/ja953491+

[59] S. Lin, Y. Zhao, Z. Ji, J. Ear, C.H. Chang, H. Zhang, C. Low-Kam, K. Yamada, H. Meng, X. Wang, R. Liu, S. Pokhrel, L. Mädler, R. Damoiseaux, T. Xia, H.A. Godwin, S. Lin, A.E. Nel, Small 9 (2013) 1776-1785. https://doi.org/10.1002/smll.201202128

[60] S. Lin, Y. Zhao, T. Xia, H. Meng, Z. Ji, R. Liu, S. George, S. Xiong, X. Wang, H. Zhang, S. Pokhrel, L. Mädler, R. Damoiseaux, S. Lin, A.E. Nel, ACS Nano 5 (2011) 7284-7295. https://doi.org/10.1021/nn202116p

[61] K.M. Fukasawa, T. Hata, Y. Ono, J. Hirose, J. Amino Acids 2011 (2011) 574816. https://doi.org/10.4061/2011/574816

[62] F.X. Gomis-Ruth, F. Grams, I. Yiallouros, H. Nar, U. Kusthardt, R. Zwilling, W. Bode, W. Stocker, J. Biol. Chem. 269 (1994) 17111-17117. https://doi.org/10.2210/pdb1iaa/pdb

[63] P. Kumari, P.K. Panda, E. Jha, K. Kumari, K. Nisha, M.A. Mallick, S.K. Verma, Sci. Rep. 7 (2017) 16284. https://doi.org/10.1038/s41598-017-16581-1

[64] T.H. Chen, C.C. Lin, P.J. Meng, J. Hazard. Mater. 277 (2014) 134-140. https://doi.org/10.1016/j.jhazmat.2013.12.030

[65] X. Zhu, J. Wang, X. Zhang, Y. Chang, Y. Chen, Nanotechnol. 20 (2009) 195103. https://doi.org/10.1088/0957-4484/20/19/195103

[66] S. Kashiwada, Environ Health Perspect. 114 (2006) 1697-1702. https://doi.org/10.1289/ehp.9209

[67] J. Duan, Y. Yu, H. Shi, L. Tian, C. Guo, P. Huang, X. Zhou, S. Peng, Z. Sun, PLoS ONE 18 (2013) e74606. https://doi.org/10.1371/journal.pone.0074606

[68] K.J. Ong, X. Zhao, M.E. Thistle, T.J. Maccormack, R.J. Clark, G. Ma, Y. Martinez-Rubi, B. Simard, J.S.C. Loo, J.G.C. Veinot, G.G. Goss, Nanotoxicol. 8 (2014) 295-304. https://doi.org/10.3109/17435390.2013.778345

[69] K.-T. Kim, R.L. Tanguay, Environ. Health Toxicol. 29 (2014) e2014021. https://doi.org/10.5620/eht.e2014021